JOURNAL OF GEOPHYSICAL RESEARCH, VOL. 103, NO. B4, PAGES 7293–7313, APRIL 10, 1998

Fracture zone subduction and reactivation across the Puysegur ridge/trench system, southern New Zealand

Jean-Frédéric Lebrun

University Paris VI, Villefranche sur mer, France

Garry D. Karner

Lamont-Doherty Earth Observatory, Palisades, New York

Jean-Yves Collot

ORSTOM, Institut Français de Recherche Scientifique pour le Développement en Coopération, Villefranche sur mer France

Abstract. A two-dimentional kinematic model for lithospheric thrusting that considers the flexural interaction between the underriding and overriding plates was used to assess the mechanical implications of subducting trench-parallel fracture zones on the topography and free-air gravity anomalies of the Puysegur ridge/trench system. Fracture zones in the underriding plate are simulated by vertical discontinuities across which bending and shearing stresses cannot be supported. The implication of reactivating fracture zones on the outer trench slope is to suppress the flexural bulge, creating topographic relief between the fracture zone and the trench, and reducing the trench gravity anomaly. In the studied region the trench subparallel L'Atalante fracture zone accounts for the lack of a flexural bulge, strong outer trench slope, and gravity gradients. The southward decrease of the trench fracture zone distance results in a decrease of the trench gravity anomaly. The effect of subducting and vertically reactivating fracture zones within the underriding plate is to segment the load of the overriding plate, creating a trough located above the underthrust fracture zone. The vertical offset and gravity modifications are functions of the fracture zone position relative to the trench. This model explains the 3500-m-deep troughs and the 1700-m subsidence observed at the Puysegur ridge. We speculate that reactivating underthrust fracture zones can facilitate strike slip faults development within the upper plate in case of oblique subduction and are conducive to the formation and dispersion of terranes at convergent margins. This process can account for basal tectonic erosion.

1. Introduction

Oceanic fracture zones are areas of mechanical discontinuity in the lithosphere that can be tectonically reactivated when subjected to horizontal and vertical stresses. Fracture zones that are involved in subduction zones may therefore have a considerable influence on the topographic and structural development of the trench and forearc regions of convergent margins. This fracture zone influence depends upon a number of parameters, including the age of the lithosphere either side of the fracture zone, the topographic variation across the fracture zone, and the fracture zone length and orientation with respect to the trench.

Fracture zones that trend suborthogonally to the trench and are subducted at a large angle to the trench tend to be relatively common. For example, as shown by *Moore and Sender* [1995], the subducted Panama fracture zone disrupts the accretionary prism in a major way. *Cande et al.* [1987] proposed that the Taitao fracture zone of southern Chile is reactivated as a tear fault and thus has the potential of disrupting the continental margin as it is subducted. The development of the Mexican Colima rift and the Manzanillo trough on the upper North American plate coincides spatially with the presence of the subducted Riviera fracture zone. This fracture zone was reactivated as a tear fault by the divergent movement of the Riviera and Cocos plates [*Stock and Lee*, 1994; *Bandy et al.*, 1995]. Subduction of the Mendocino fracture zone has significantly altered the topography of the North America plate margin. This process is responsible for a differential elevation (500-1000 m high) of the overriding plate either side of the fracture zone trace [*Glazner and Schubert*, 1985].

In contrast, fracture zones that trend subparallel to trenches are less well studied, and so their effects on convergent margins are poorly understood. South of New Zealand, the oceanic crust that straddles the Macquarie Ridge Complex along the Pacific/Australia convergent plate boundary contains a number of fracture zones that trend subparallel to the plate boundary (Figure 1). These fracture zones are recognized from satellite gravity anomalies [*Sutherland*, 1995] and swath bathymetric data recently acquired east and west of the Macquarie Ridge Complex [*Coffin et al.*, 1994] and west of the Puysegur ridge [*Collot et al.*, 1995b; *Delteil et al.*, 1996] (Figure 1). *Karner et al.*

Paper number 98JB00025.
0148-0227/98/98JB-00025$09.00

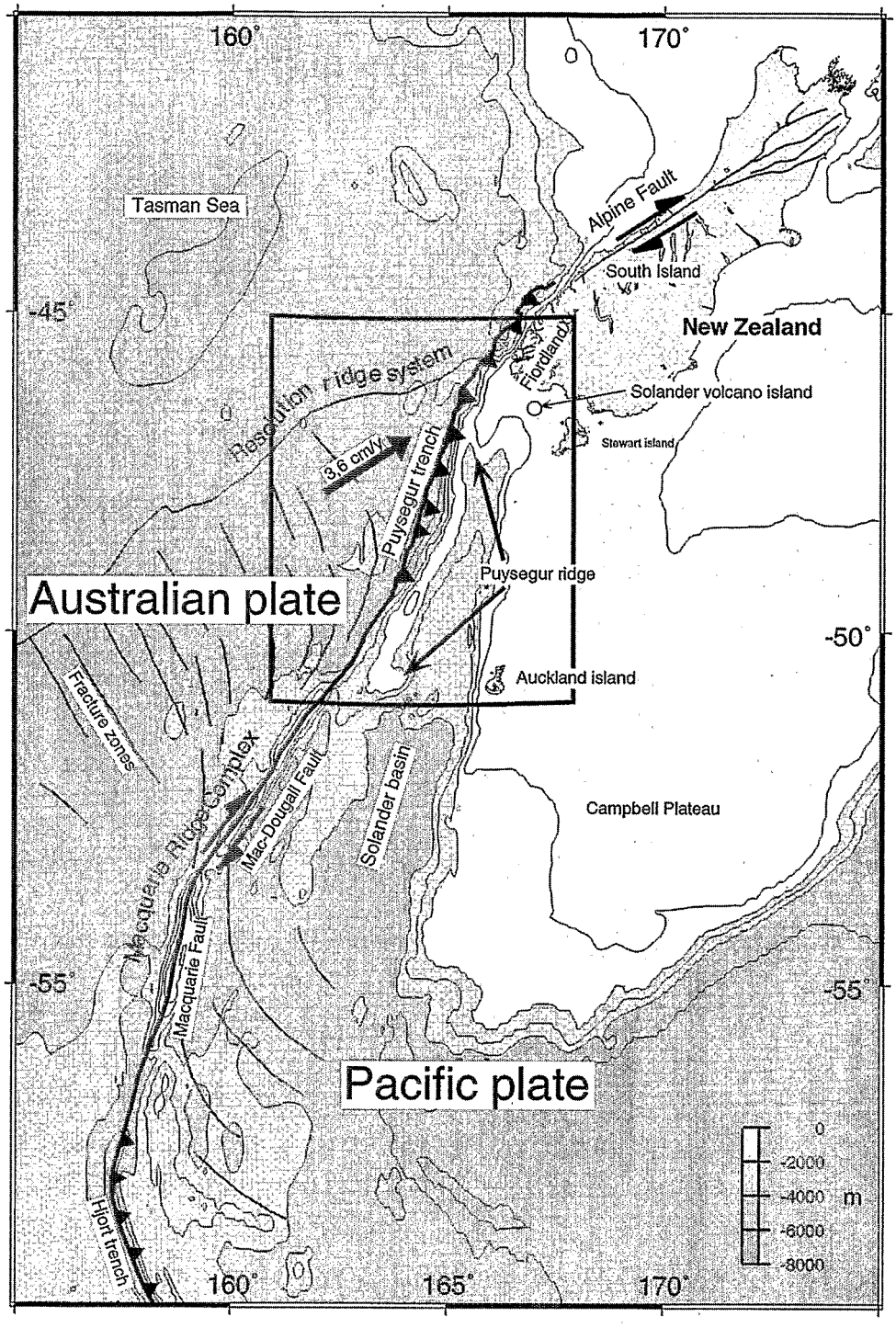

Figure 1. (Opposite) Location map of the Puysegur ridge/trench system and its structural relationship to the Macquarie Ridge Complex (MRC). The MRC can be divided into several segments along which varying amounts of convergence have occurred between the Australian and Pacific plates. The northernmost part of the MRC, the Puysegur ridge, is associated with an east dipping Benioff zone. Beneath the South Island of New Zealand, both shallow and intermediate earthquakes ranging in depths from approximately 5 to 160 km have been recorded, and the extrusion of calc-alkalic volcanics on Solander Island to the east of Puysegur trench confirm that subduction has occurred. Subduction is oblique, with a convergence angle of approximately 30°. The Resolution ridge separates the northern, mostly Cretaceous crust of the Tasman Sea from the southern, entirely Cenozoic crust. Convergence trajectories are calculated using the NUVEL-1A pole of rotation from *De Mets et al.* [1994]. Bathymetric contour interval is 500 m. The frame shows location of Figures. 2 and 5. Note the Cenozoic fracture zones on both the Pacific and Indo-Australian plates that asymptotically approach the MRC.

[1994] used gravity and topographic profiles to show that fracture zones adjacent to the Macquarie ridge have strongly affected the morphology of the ridge. Along the Fiordland margin of New Zealand, the plate boundary is an oblique, eastward dipping subduction zone characterized by a 150-km-deep Benioff zone [*Smith*, 1971; *Davey and Smith*, 1983; *Reyners*, 1989] that becomes nascent along the Puysegur ridge and trench [*Ruff et al.*, 1989; *Anderson and Webb*, 1994]. The Solander Volcano (Figure 1) is the only quaternary andesitic volcano associated with this subduction [*Reay*, 1986]. The purpose of this paper is to model the observed topography and gravity of the Puysegur ridge/trench system in a region where trench-parallel fracture zones have been progressively underthrust (i.e., subducted) using a kinematic model for lithospheric thrusting that explicitly considers the flexural interaction between both the overriding and underriding plates.

2. Geodynamic Setting

The Macquarie Ridge Complex traverses a wedge of Cenozoic oceanic crust that lies south of Fiordland, New Zealand (Figure 1). Oceanic spreading occurred in this region after the Cretaceous Tasman Sea oceanic crust and the western continental margin of the Campbell Plateau rifted [*Sutherland*, 1995]. Initial Eocene spreading generated fracture zones perpendicular to the rifted margin [*Weissel and Hayes*, 1977; *Kamp*, 1986]. During the late Oligocene to early Miocene the fracture zones started to rotate clockwise in conjunction with the southeastward migration of the Pacific-Australian pole of rotation [*Walcott*, 1978; *Sutherland*, 1995; *Lamarche et al.*, 1997]. Segments of fracture zones created during the Neogene [*Massell et al.*, 1995; *Lamarche et al.*, 1997] formed parallel to the plate boundary and were offset by 330 km of dextral movement when the plate boundary became dominantly strike slip [*Massell et al.*, 1995; *Lamarche et al.*, 1997].

Oblique northeastward subduction initiated beneath Fiordland about 10 Ma [*Davey and Smith*, 1983] and started to propagate southward along an oceanic fracture zone at approximately 5-10 Ma as a consequence of the westward migration of the pole of rotation [*Collot et al.*, 1995b]. This subduction has resulted in the removal of about 350 km of crust. *Christoffel and Van der Linden* [1972] proposed that the downgoing slab is shaped like an "inverted plough," with virtually no subduction of crust along the southern Puysegur ridge. *Collot et al.* [1995b] demonstrated, however, that incipient underthrusting occurs at the western toe of the southern part of ridge and that strike slip motion occurs along its summit.

Along the northern part of the Puysegur trench, upper Eocene oceanic crust of the Australian plate has been subducted, whereas in the south, crust as young as mid Miocene has been subducted [*Wood et al.*, 1996]. The maximum depth of the trench is located at 48°15'S and reaches -6200 m (Figure 2). The L'Atalante fracture zone is located due west of the plate boundary and can be traced from 50°20'S [*Coffin et al.*, 1994], where it coalesces with a strike slip segment of the plate boundary, to 48°45'S where the fracture zone becomes buried by sediments [*Collot et al.*, 1995b]. Between 49°45'S and 48°45'S, the L'Atalante fracture zone is located 17-30 km west of the Puysegur trench and trends subparallel to it (Figure 3). On the downgoing plate a clear flexural bulge due to the bending of the Australian plate west of the Puysegur trench cannot be distinguished in either the bathymetry or the free-air gravity data. Instead, where detailed bathymetry is available, we observe a gentle dip of the downgoing plate west of the L'Atalante fracture zone and a sharp increase in slope east of the fracture zone (Figure 3). Trench-parallel normal faults that should form within the outer trench slope during the bending and upper-crustal brittle failure of the Australian plate are rare. Normal faults do appear, however, east of the L'Atalante fracture zone, and they become more numerous towards the north [*Delteil et al.*, 1996].

The Puysegur ridge has a relief of nearly 6 km and an along-strike length of 350 km from 50°30'S to 47°S where it merges with the continental margin of New Zealand (Figure 2). Using geophysical data, *Collot et al.* [1995b] suggested that the ridge consists mainly of deformed oceanic crust and ophiolite rocks. Basalts and serpentinites dredged from ridge scarps supports this interpretation [*Summerhayes*, 1969; *Mortimer*, 1995]. Swath bathymetric data indicate that the ridge broadens and deepens northward. The southern part of the ridge is less than 50 km wide, whereas in the north the width is 80 km (Figures 2 and 4). The ridge summit is dissected by the Puysegur strike slip fault that trends N26°E from 50°S to 48°S. The fault trace extends along a 1500-2000 m below sea level, 2-5 km wide axial valley flanked to the east by the ridge summit and to the west by a secondary, deeper crest (Figure 4, profiles 1 and 2). From 48°S northward, the strike slip fault splays into several branches bounding elongated, 3250 to 3800-m-deep 10 to 20-km-wide basins collectively termed the Puysegur trough [*Delteil et al.*, 1996] (Figure 4, profiles 3, 4, and 5). This trough trends N10°E, oblique to the N26°E direction of the Puysegur Fault and splits the ridge into two major summits. The tectonic origin of the Puysegur trough has remained controversial. During subduction initiation, transverse extension along the strike slip fault zone may have been responsible for the origin of the trough [*Collot et al.*, 1994]. In this paper, we show that the trough formation could also have been influenced by the reactivation of a subducted fracture zone.

In the south the summit of the ridge consists of discrete flat-topped segments, the southernmost of which is close to sea level (-120 m) at 49°30'S and is interpreted to be the result of subaerial exposure and erosion [*Collot et al.*, 1995b]. The ridge summit shows other individual flat tops that lie northward at progressively greater depth (-675 m at 48°50'S and -1800 m at 47°45'S; Figure 4). The northward increase in the depth of the ridge flat tops implies 1700 m of subsidence of the ridge. These morphostructural data together with earthquake focal mechanisms have been interpreted by *Collot et al.* [1995b] to be the result of differential uplift, subsidence, and trenchward collapse of a ridge that formed by transpression along the plate boundary during subduction initiation. Where subduction is incipient, for example, in the southern Puysegur ridge/trench system, large horizontal stresses have induced subaerial exposure of the ridge. As this in-plane compression is released due to interplate decoupling (i.e., subduction), the ridge broadens and collapses (e.g., along the northern part of the Puysegur ridge).

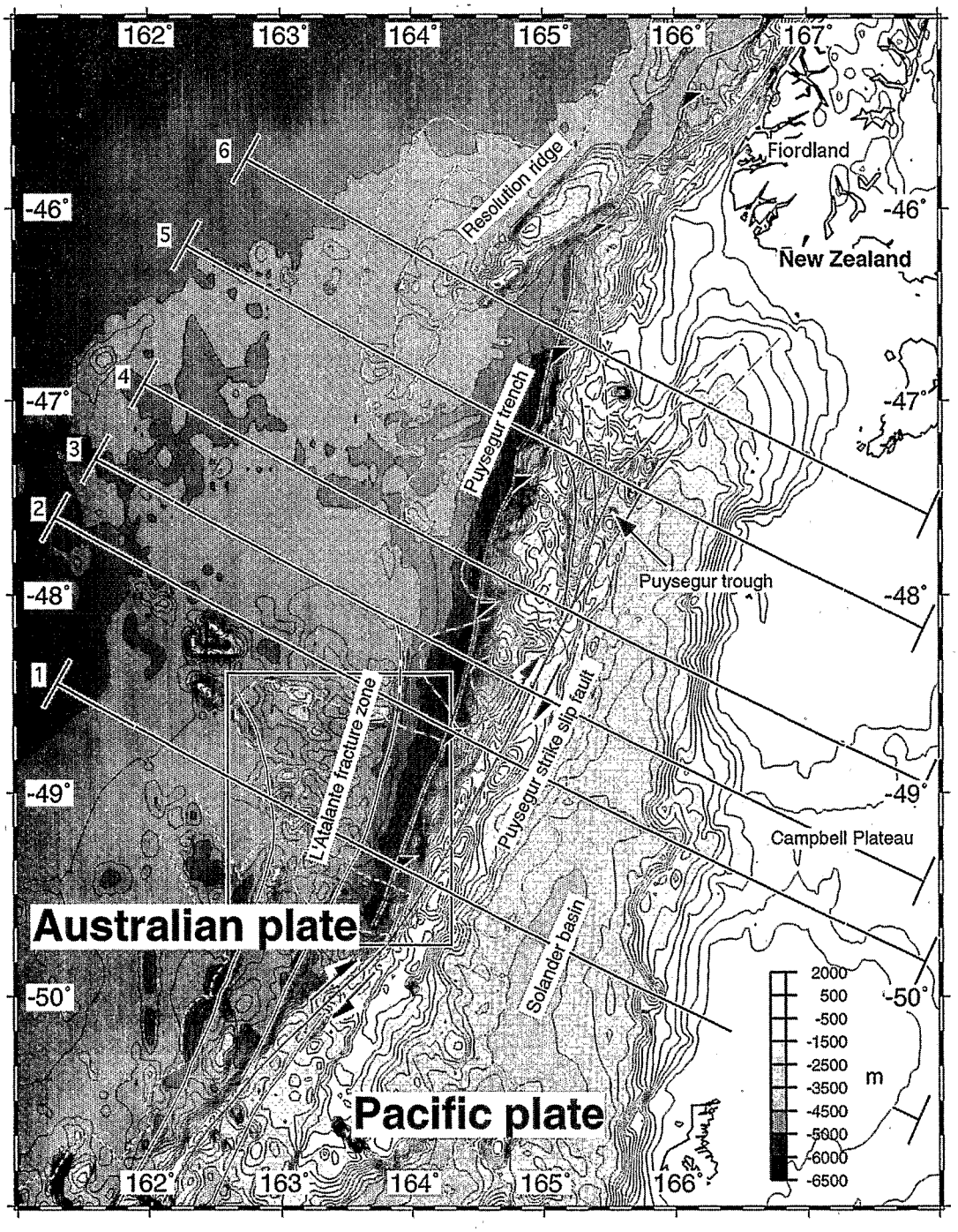

Figure 2. Bathymetric map along the Puysegur ridge/trench system and location of profiles 1-6 presented in Figure 12. Thin dashed line represents areas surveyed during the Geodynz-sud, R/V *L'Atalante* [*Collot et al.*, 1995a], and R/V *Rig Seismic* [*Coffin et al.*, 1994] cruises on the Macquarie Ridge Complex. Thick lines are major active fault zones and Cenozoic fracture zones. Bathymetric contour interval is 250 m. Frame shows location of Figure 3.

Figure 3. Bathymetric cross sections across the L'Atalante fracture zone (AFZ) stacked on the Puysegur trench. Dotted lines represent the predicted flexure of thin continuous elastic plate with an effective elastic thickness of 15 km. Inset: Detailed bathymetry along the L'Atalante fracture zone and location of cross sections 1-5. Regions of light shading represent prominent topographic highs, whereas zones of heavy shading correspond to prominent topographic lows.

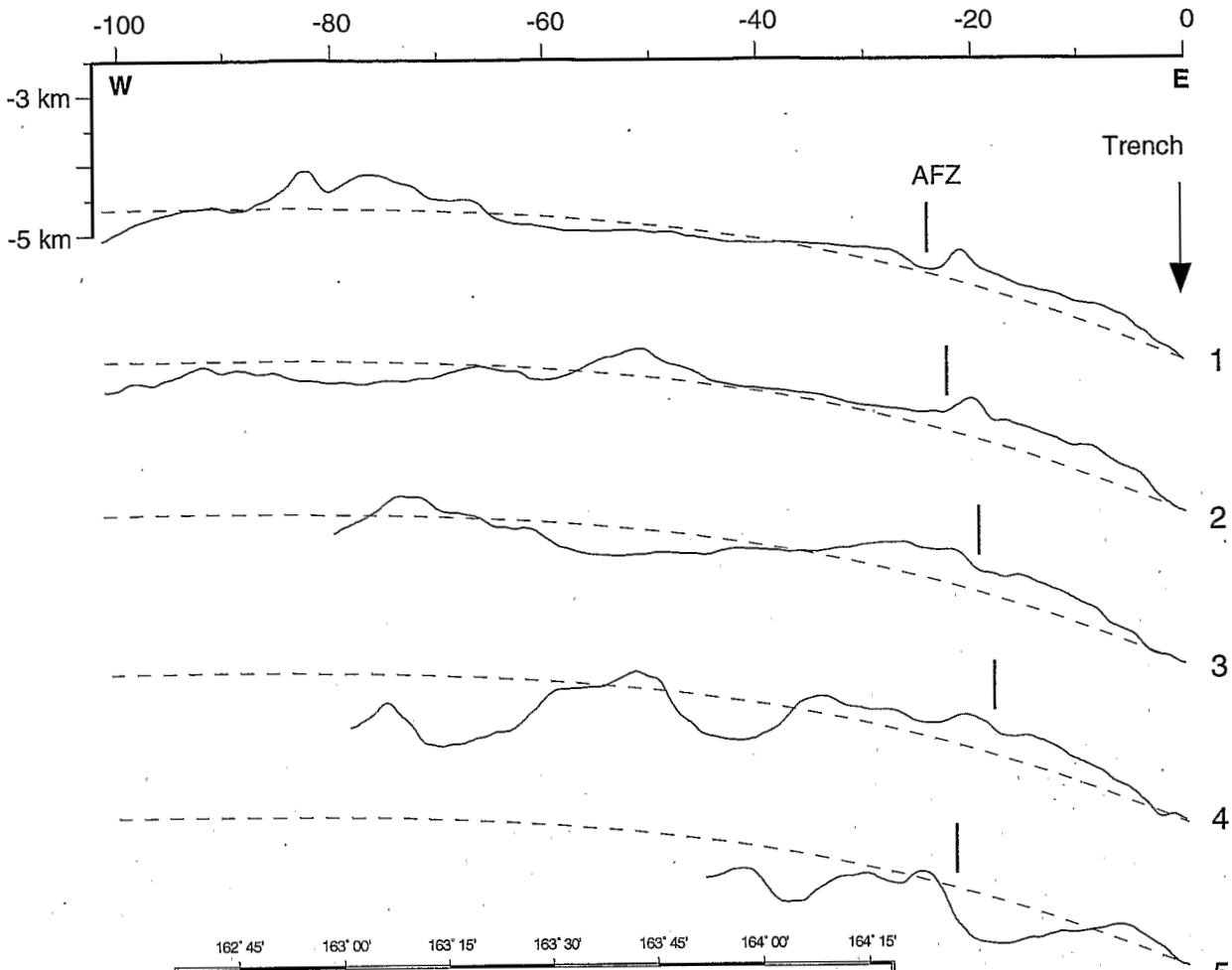
-100
-80
-60
-40
-20
0
W
E
-3 km
-5 km
Trench
AFZ
1
2
3
4
5

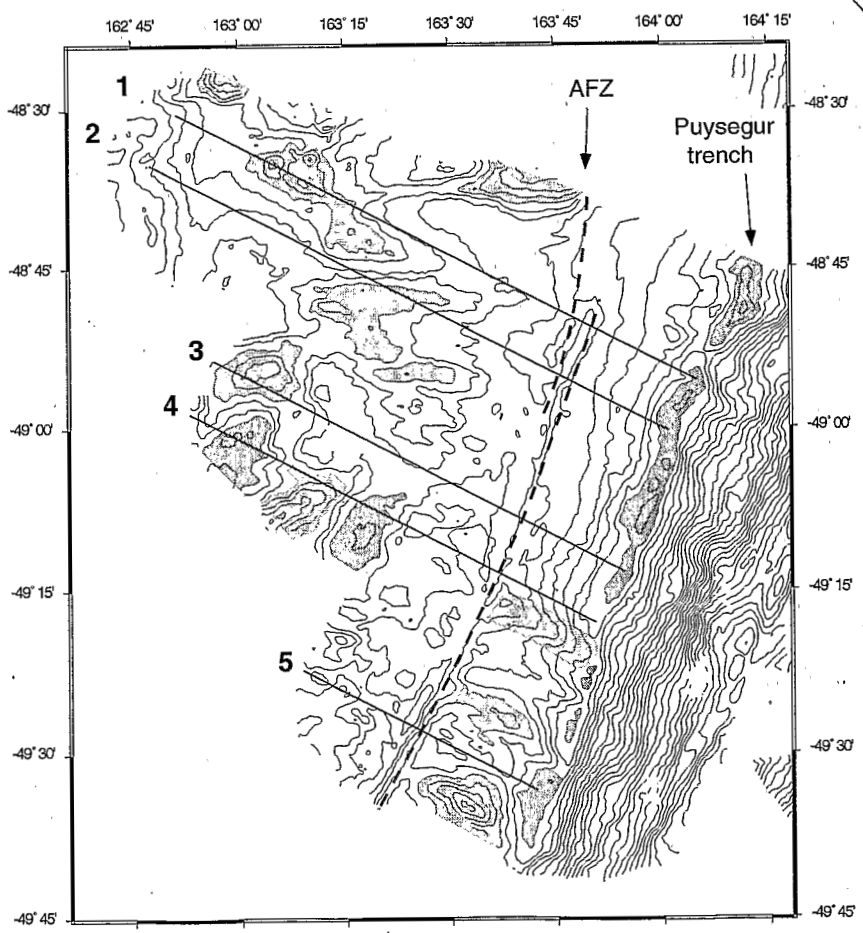
162° 45'
163° 00'
163° 15'
163° 30'
163° 45'
164° 00'
164° 15'
-48° 30'
-48° 45'
-49° 00'
-49° 15'
-49° 30'
-49° 45'
1
2
3
4
5
AFZ
Puysegur
trench

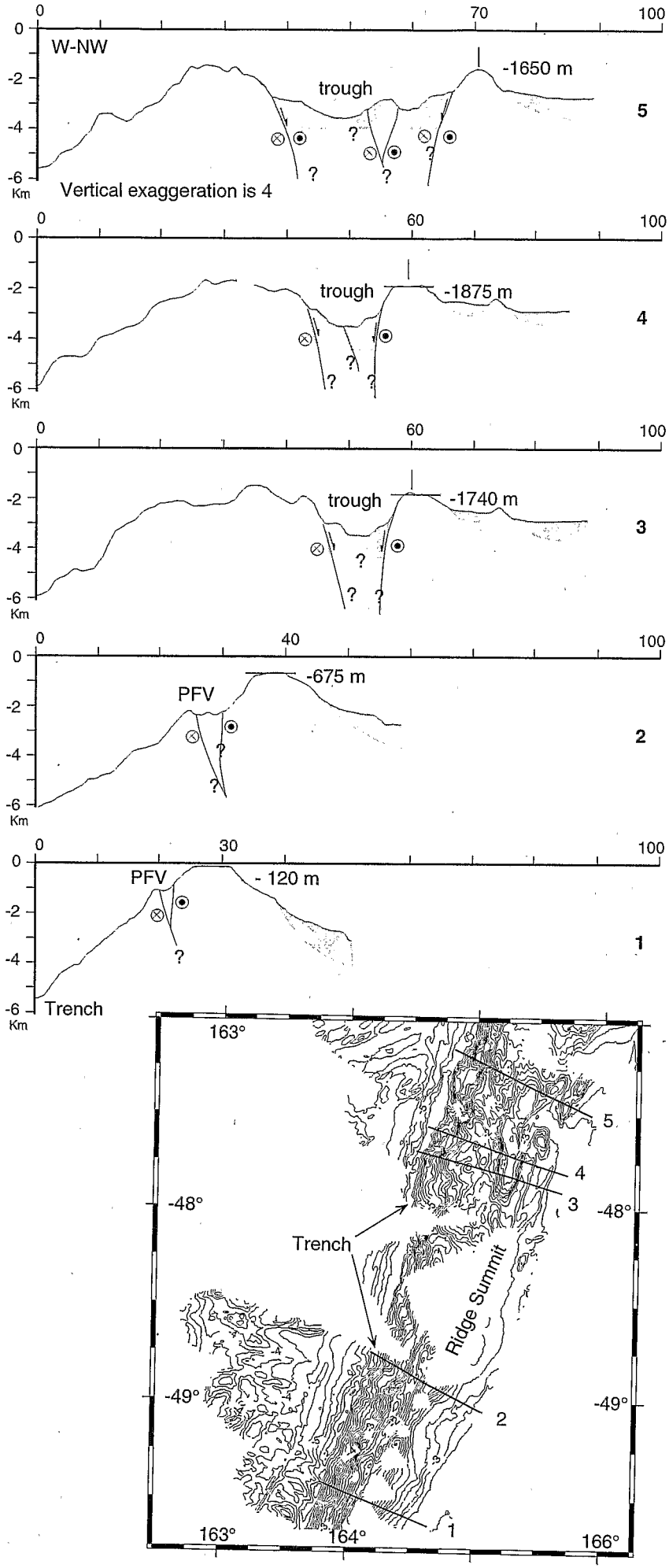
0
70
100
W-NW
-1650 m
trough
5
Vertical exaggeration is 4
Km
60
-1875 m
4
-1740 m
3
40
-675 m
PFV
2
30
- 120 m
1
Trench
163°
-48°
-49°
Ridge Summit
164°
166°

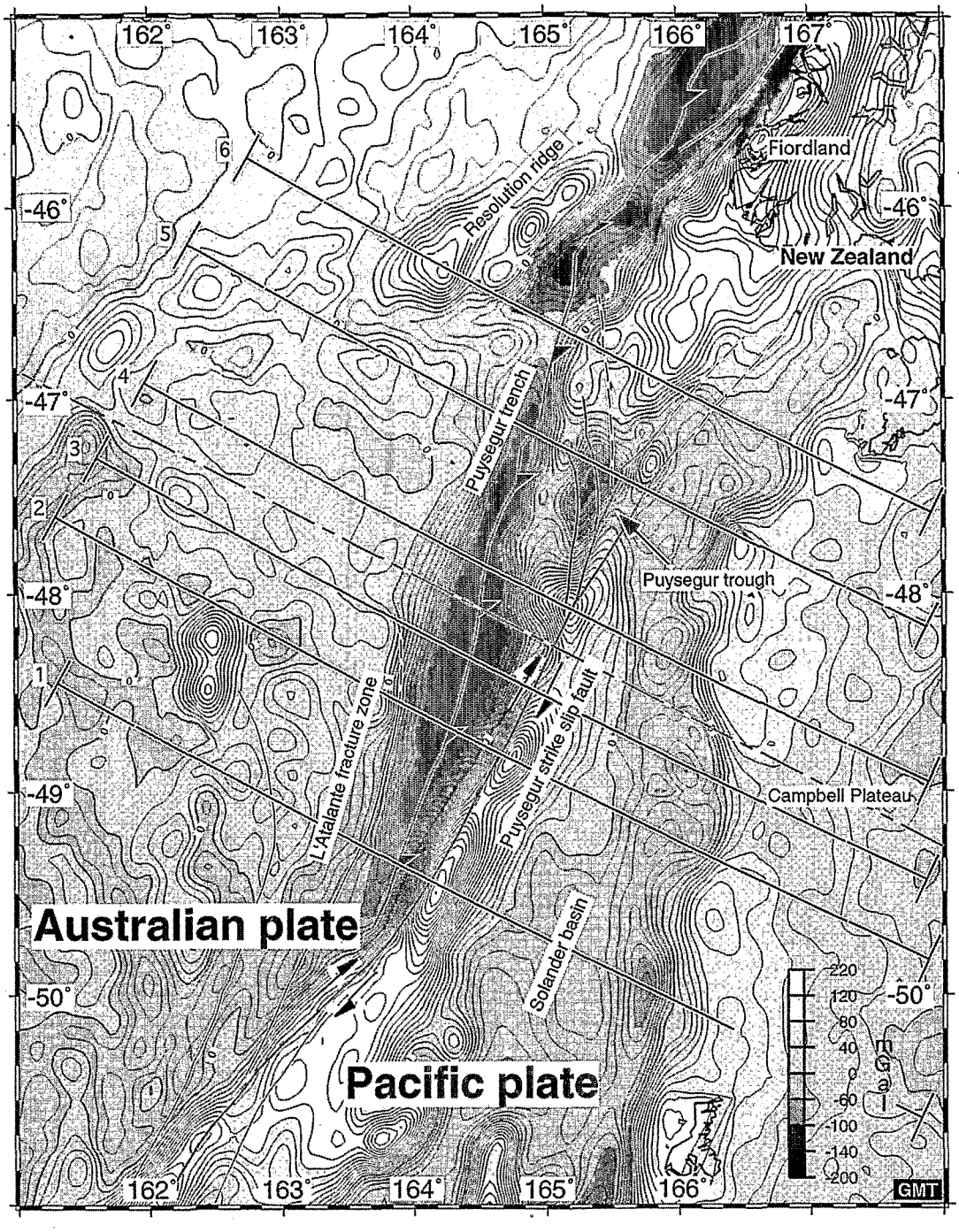

Figure 5. Free-air gravity anomaly map of the Puysegur ridge/trench system determined using shipboard measurements and the satellite-derived gravity map [*Sandwell and Smith*, 1994]. Profiles 1-6 are presented on Figure 12. Thick lines are major active fault zones and Cenozoic fracture zones. Thin line delimits the northern and southern domain of the ridge-trench system. Gravity contour interval is 10 mGal.

Figure 4. Bathymetry profiles across the Puysegur ridge stacked on the trench showing the flat tops of the ridge easternmost summit (shown by a thin horizontal line with depth value), the ridge-trench distance that increases from 30 km in profile 1 to 70 km in profile 5, the Puysegur Fault Valley (PFV) on profiles 1 and 2 that changes to a trough dividing the ridge into western and eastern summits on profiles 3 to 5. Shaded region corresponds to regions of sediment accumulation as interpreted from seismic reflection profiles obtained during Geodynz-sud Cruise of R/V *L'Atalante* [*Collot et al.*, 1995a]. Inset : Location of the bathymetric profiles. Contour interval is 250 m. Depth annotation in kilometers.

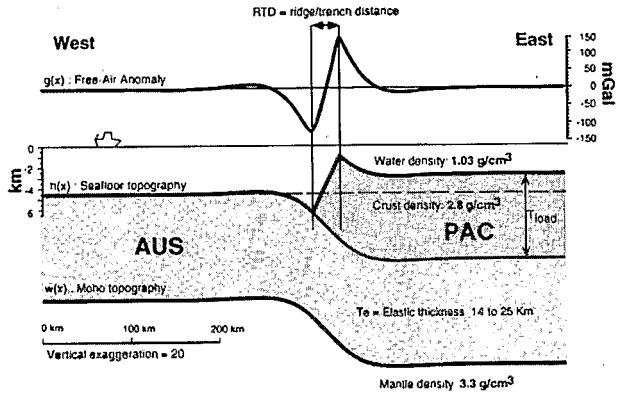

Figure 6. Schematic representation of the kinematic and flexural model used to model the Puysegur ridge/trench system and corresponding resulting free-air gravity.

3. Free-Air Gravity Anomalies Over the Puysegur Ridge and Trench

Free-air gravity anomalies associated with the Puysegur ridge and trench can be separated into two geographic domains based on their wavelength and amplitude characteristics. South of about 48°S (the southern domain), there is a dipole relationship between the positive and negative gravity anomalies (Figure 5). The minimum gravity value varies from -70 mGal at 49°30'S to -180 mGal at 48°10'S with a corresponding increase in anomaly width from 20 to 80 km . On the downgoing plate, the western flank of this anomaly shows a sharp increase in gradient associated with the L'Atalante fracture zone. The positive free-air gravity anomaly associated with the Puysegur ridge peaks at 215 mGal at 49°30'S and decreases northward to about 170 mGal at 48°45'S and 100 mGal at 48°10'S. The secondary crest of the Puysegur ridge has no specific gravity signature.

In the northern domain where the ridge divides in two summits separated by the Puysegur trough, the free-air gravity is mainly negative, and both ridge summits and the trough are associated with a characteristic gravity anomaly. Near 47°30S the free-air anomaly of the western summit is approximately -40 mGal with the eastern summit showing a range from +30 to -30 mGal. Over the Puysegur trough, the free-air gravity reaches a minimum value of -110 mGal. This gravity low extends northward into the southern margin of New Zealand. The elongation of the low is associated with a slight depression in the margin topography. The Puysegur trench free-air gravity anomaly over the northern domain has a smaller amplitude and width compared with the trench free-air gravity immediately south of 48°S.

4. Models of Lithospheric Flexure

In this paper we consider a mechanical model in which the Puysegur ridge is supported by the elastic strength of the down-flexured Australian plate. In particular, we use a two-dimentional (2-D) kinematic model for lithospheric thrusting that explicitly considers the flexural interaction between both the overriding and underriding plates (Figure 6). Flexural isostasy is calculated assuming elastic thin plate theory [e.g., *Gunn*, 1943; *Walcott*, 1970]. Inasmuch as the subduction is incipient, that is, there is no slab pull, we consider that the deflection of the Australian plate along the Puysegur trench results from the vertical and horizontal loads emplaced during the overthrusting of the Pacific plate (Figure 7). In this model, while we can include the effects of the horizontal forces that arise from the initiation of subduction, we find that these forces are minor compared to the vertical forces deforming the Australian and Pacific plates across the plate boundary.

The deflection of the lower plate $\omega(x)$ in response to overthrusting is given by the following differential equation for the flexure of an elastic plate overlying a fluid [e.g., *Turcotte*, 1979]:

$$D\frac{\partial^4 \omega(x)}{\partial x^4} + (\rho_m - \rho_w) g \omega(x) = (\rho_{load} - \rho_w) g T_{load}(x) \quad (1)$$

where $T_{load}(x)$ is the crustal thickness of the upper plate, g is the acceleration due to gravity, ρ_m is the density of the material underlying the plate, ρ_{load} is the load density

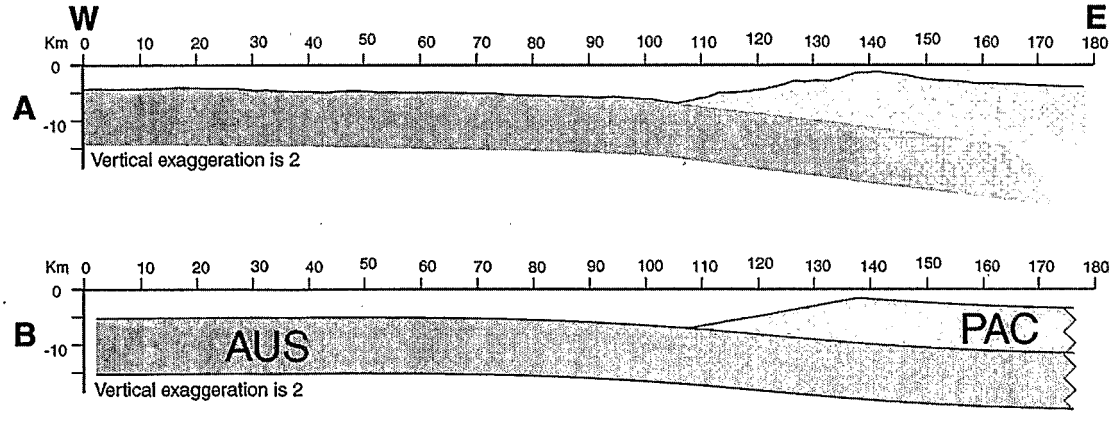

Figure 7. (a) Possible positions of the slab beneath the Puysegur ridge where subduction is poorly developed (i.e., southern Puysegur trench). The Australian plate is flexed under the load of the Pacific plate. (b) Simple model of loading used to represent the Puysegur ridge/trench system. Both sections are at the same scale and aligned along the trench. Light stipple represents Pacific crust, while the dark stipple represents crust of the Australian plate.

(assumed to be the crustal density of the upper plate), and ρ_W is the density of the material infilling the deformation (assumed to be seawater). D is the flexural rigidity defined by

$$D = \frac{ETe^3}{12(1-\nu^2)}$$

where Te is the effective elastic thickness of the lithosphere, E is Young's modulus, and ν is Poisson's ratio. The final or resultant topography/bathymetry $h(x)$ is determined by adding $T_{load}(x)$ and $\omega(x)$ (Figure 6).

Fracture zones in the underriding plate are simulated by a vertical discontinuity across which bending and shearing stresses cannot be supported. We calculate the bending and shearing stresses in a continuous plate and, at the location of the plate fracture or discontinuity, we apply an opposing bending moment and shearing force. Because ages of the oceanic crust and positions of the paleospreading centers on either side of the plate boundary are poorly constrained, we assume that the crustal and effective elastic thicknesses of the plate either side of the fracture zone is the same. The resulting free-air gravity associated with the modeled flexed system is calculated using the Fourier transform method of *Parker* [1972]. The free-air gravity is the resultant effect of density contrasts represented by the deformed surface and Moho topographies (relative to their undeformed configurations).

The modeled free-air gravity and topography depend on the density and thickness of the Australian and Pacific crusts. The crust on either side of the Puysegur ridge is oceanic, with the ridge summit lying below sea level. We used a crustal density of 2800 kg/m^3, a water density of 1030 kg/m^3, and a mantle density of 3300 kg/m^3. We neglected the sediments infilling the trench because they are rather sparse in this region [*Delteil et al.*, 1996]. The upward continuation distance of the crust/water interface is fixed at an average value of 4.5 km, whereas the upward continuation value for the crust/mantle interface is fixed at an average value of 12.5 km.

We assume that the thickness of the Pacific crust defines the load applied to the Australian plate, increasing from 0 at the trench to a maximum value of T_{load} beneath the ridge summit (Figure 6). As will be shown later, the distance between the trench and the ridge summit (the ridge-trench distance) is an important parameter that partly controls the water depth of the Puysegur ridge. Where the ridge has two summits, the eastern one that shows evidence of wave-base erosion, and therefore was the main summit prior to subsidence, was chosen to define the ridge-trench distance. The ridge-trench distance along the Puysegur ridge varies from 30 km at 49°30'S to 70 km at 47°00'S (Figure 4). As the Pacific crust is overthrust, the hanging wall collapses to form a wedge of crustal material that extends from the trench to the ridge summit. In general, the décollement has not been imaged and its dip is unknown. The inner trench slope shape is a function of both the collapsed shape of the hanging wall block and accretionary processes within the trench and frontal forearc crust. Along the northern Puysegur trench, the inner slope has been molded into a convex shape by tectonic erosion [*Delteil et al.*, 1996]. Given these trench-modifying complexities, we assume that the thickness of the forearc wedge increases linearly from the trench to a maximum value of T_{load}. By doing so, we are possibly underestimating the wedge load and thus the predicted ridge depth is a minimum (Figure 8).

The maximum thickness of the crust east of the ridge summit is not known directly from marine geophysical measurements. We have chosen a thickness of 8 km because this value is typical of average oceanic crustal thicknesses [*White et al.*, 1992] and provides a calculated topography that fits well with the observed. An error in the crustal thickness by a few kilometers may change the amplitude of the gravity anomaly by several tens of mGal (Figure 9 and Table 1) but does not affect the wavelength of the calculated gravity.

Another important parameter controlling the wavelength and shape of the modeled gravity and topography is the effective elastic thickness (Te) of the deflected underthrust and overthrust plates. *Bodine et al.* [1981] demonstrated a close relationship between the flexural strength of the lithosphere and the age of the oceanic crust. We have used this empirical relationship to calculate the value of Te for the Australian and Pacific plates involved in transpression across this segment of the Macquarie Ridge Complex. The age of the Australian plate along the Puysegur trench ranges between 14 and 35 Ma from south to north [*Wood et al.*, 1996], implying a range of effective elastic thicknesses from 15 to 24 km, respectively.

5. Results: Modeling the Flexure of a Continuous Plate

To investigate the implications of subducting and reactivating fracture zones on the topography and gravity of a ridge-trench system, it is first necessary to model the response of a continuous plate to characterize the flexural

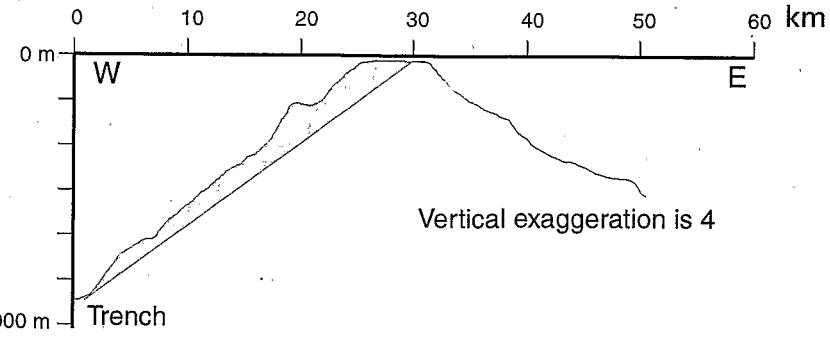

Figure 8. Linear representation of the topography comprising the inner trench slope of the Puysegur trench. By doing so, we underestimate the load of the wedge on the deflected plate (shaded area).

Table 1. Parameters and Results of Calculation for Models Presented in Figures 9, 10, 12, and 13.

Model	Figure	*T*load, km	RTD, km	*Te*, km	Fault Position, km Relative to the Trench. (Negative Numbers Westward From the Trench)	Gravity, mGal						Bathymetry, m					
						West Maximum (Trench-ward)	Central Trough	East or Single Maximum	Trench	Amplitude	Wavelength of Negative Anomalie, km	Westward Summit	Central Trough	East or Single Summit	Trench	Variation of Summit Depth Relative to Reference, m	Variation of Trench Depth Relative to Reference, m
Variation of Thickness of the Upper Plate, Tload																	
1	9.1	6	30	15	none			125.6	-108.7	234.3	87			2890	-1511	-963	507
2	9.2	8	30	15	none			180.2	-144.8	325.0	87			3853	-2018	ref=0	ref=0
3	9.3	10	30	15	none			244.4	-181.2	425.6	87			4817	-2518	964	-500
Variation of the Ridge-Trench Distance (RTD)																	
4	10A3	8	30	15	none			180.2	-144.8	325.0	87			3853	-2018	ref=0	ref=0
5	10A2	8	50	15	none			138.3	-116.2	254.5	91			3352	-1493	-501	525
6	10A1	8	70	15	none			104.3	-91.4	195.7	97			2952	-1103	-901	915
Variation of the Elastic Thickness (Te)																	
7	10B1	8	30	15	none			180.2	-144.8	325.0	87			3853	-2018	ref=0	ref=0
8	10B2	8	30	20	none			201.3	-158.7	360.0	101			4072	-2184	219	-166
9	10B3	8	30	24	none			224.0	-161.3	385.3	133			4288	-2211	435	-193
Variation of Fault Position; Fault Westward of the Trench																	
10	12.4	8	30	15	-15			164.4	-124.2	288.6	30 **			3672	-1819	-181	199
11	12.3	8	30	15	-45			164.4	-131.0	295.4	60 **			3677	-1905	-176	113
12	12.2	8	30	15	-60			167.4	-146.4	313.8	75 **			3672	-2088	-181	-70
Variation of Fault Position; Fault Eastward of the Trench																	
13	13.1	8	60	21	20	14.9	-91.1	78.7	-45.4	60.3 *	74	1888	-1295	2723	-397	-615	1236
14	13.2	8	60	21	35	71.0	-60.3	45.2	-73.7	144.7 *	81	2745	-610	2282	-863	-1056	700
15	13.3	8	60	21	60	124.2	none	none	-108.7	232.9	100	3416	none	none	-1353	78	280
16	13.4	8	60	21	none			136.0	-130.0	266.0	113			3338	-1633	ref=0	ref=0

For variation of fault position, fault westward of the trench, variation of summit depth and trench depth, reference is as model of Figure 9, model 2.

*: Amplitude is calculated between the trench minimum and the western ridge summit.

**: Wavelength is controlled by the fault position.

Abbreviation ref, model used as reference. Notice that bathymetric zero is set to the average depth of the Australian plate (usually around -4500 m); thus trench depth is negative and the ridge depth is positive.

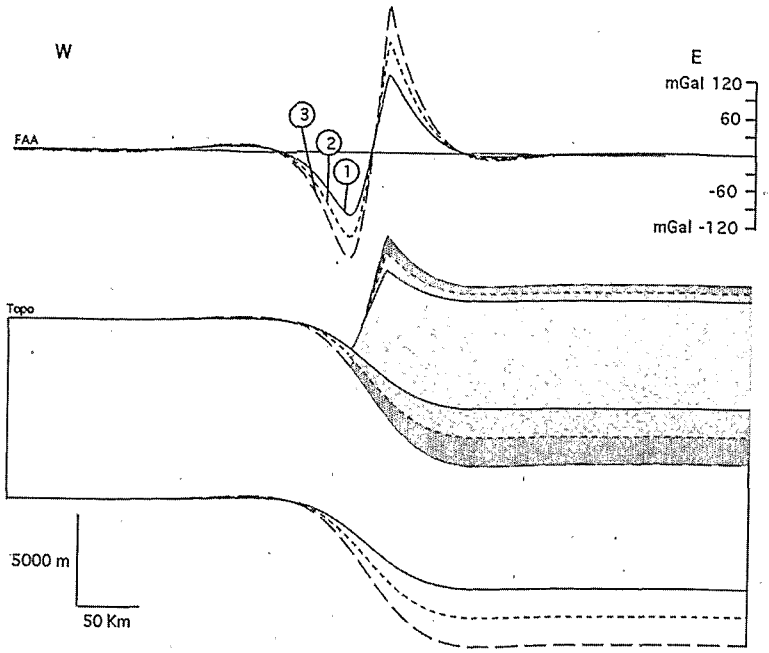

Figure 9. Effect of increasing the crustal thickness of the upper plate on the topography (topo) and the free-air gravity (FAA) of the Puysegur ridge/trench system (1, light gray, plain line, T_{load} is 6 km thick; 2, medium gray, dotted line, T_{load} is 8 km thick; 3, dark gray, dashed line, T_{load} is 10 km thick).

deformation of both the underthrust and overthrust plates and determine how the elastic thickness and ridge-trench distance control the flexural deformation. The ridge-trench distance is important because, as suggested by *Collot et al.* [1995b], the northward broadening and subsidence of the ridge is possibly related to the progressive onset of subduction along the ridge. Increasing the ridge-trench distance increases the wavelength of the free-air gravity but reduces both the amplitude of the gravity and the relief of the ridge (Figure 10a). When the ridge-trench distance increases from 30 to 50 km the ridge summit subsides by 500 m (Table 1). This value is similar to the 600 m of subsidence interpreted along the southern part of the ridge. For a ridge-trench distance of approximately 70 km (that observed for the northern part of the Puysegur ridge; Figure 4), the predicted subsidence of the ridge is 900 m. This calculated subsidence accounts for only part of the 1700 m subsidence interpreted along the northern part of the ridge.

The modeled elastic thickness of the downgoing plate increases northward, consistent with the increase in age of the Australian plate. Increasing the elastic thickness of the subducting plate increases slightly the wavelength and amplitude of the free-air gravity in addition to the relief of the ridge (Figure 10b and Table 1). Thus increasing *Te* partially counterbalances the subsidence effect associated with the ridge broadening. However, the *Te* of the underriding crust beneath a fixed point of the ridge may have varied with time, thus counterbalancing or favoring ridge subsidence. For example, *Te* of the underriding plate may have decreased beneath the ridge because progressively younger crust was being subducted (Figure 11). For crustal ages between 10 and 40 Ma, a +/-2-km error in *Te* corresponds to an age variation of about +/-6 Ma [*Bodine et al.*, 1981]. Such an error in *Te* translates into a 200-m variation in the calculated depth of the ridge summit. An estimate of the age variation of the underriding crust can be obtained using the Australian/Pacific finite rotation parameters given by *Sutherland* [1995]. We calculated an average 32 km/Ma convergence rate and an average N45° plate convergent direction during the last 10 m.y. Considering these results and that the trend of the magnetic anomalies of the underriding crust is highly oblique to the trench, we estimate that the age variation of the underriding crust beneath the ridge did not exceed 10 m.y. This maximum age variation implies a ~100-m error on the calculated ridge depth. From our modeling we conclude that with a continuous plate the maximum subsidence of the ridge due to variations of the shape of the overriding plate and the elastic thickness (*Te*) of the underriding plate accounts for a total subsidence of 900 m +/-100 m.

The continuous plate model presented above does not satisfactorily explain the evolution of the topography and gravity anomalies along the Puysegur ridge/trench system, that is, it is difficult to explain the observed 1700-m subsidence of the ridge. However, we believe that the *Te* and ridge-trench distance values used in this modeling are realistic. We will now consider flexure models in which fracture zones within the underriding plate can be reactivated in response to relieving bending stresses (Figures. 12 and 13 and MP in Table 2). To investigate the importance of fracture zones on the subduction process, we have constructed six profiles along the ridge-trench system (Figure 14). We will compare the plate-fracture models with topographic and gravity sections from across the Puysegur ridge/trench system. The reference models take into account the concurrent northward increase of the elastic thickness and ridge-trench distance along the ridge described earlier (Table 2).

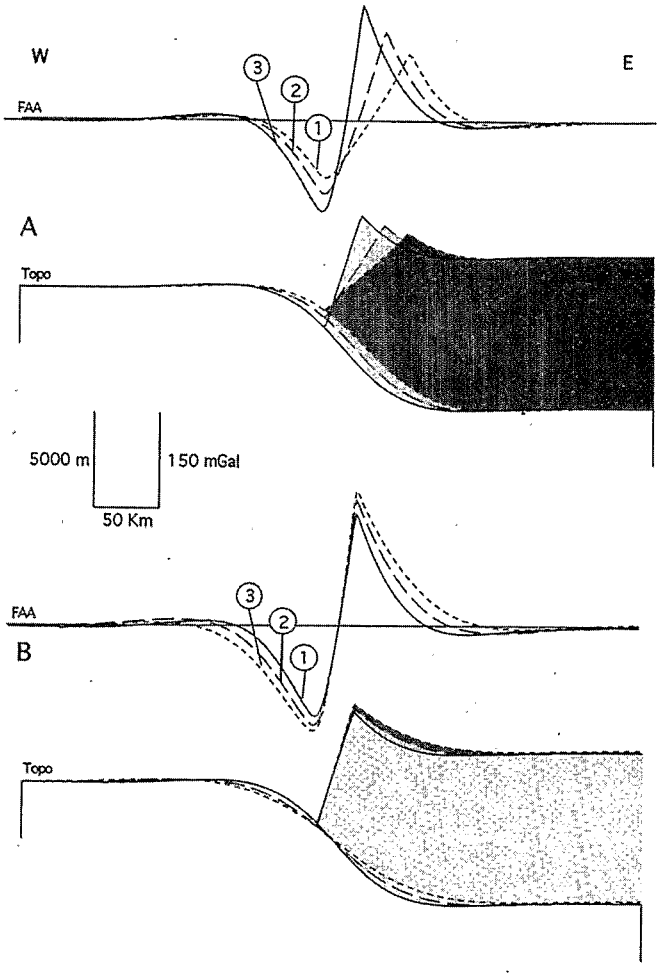

Figure 10. (a) Effect of increasing the ridge-trench distance (RTD) on the modeled topography and free-air gravity: 1, light gray, plain line, RTD is 30 km; 2, medium gray, dashed line, RTD is 50 km; 3, dark gray, dotted line, RTD is 70 km. (b) Effect of increasing effective elastic thickness on the modeled topography and free-air gravity: 1, light gray, plain line, *Te* is 15 km; 2, medium gray, dashed line, *Te* is 20 km; 3, dark gray, dotted line, *Te* is 24 km).

6. Fault Reactivation: Loading a Plate With Fracture Zones

6.1. Effect of Fracture Zones Within the Outer Trench Slope

The reactivation of fracture zones as they migrate through the flexural outer bulge of a trench system modifies the topography and free-air gravity anomaly of both the bulge and the trench but does not significantly change the ridge topography and free-air gravity (Figure 12). Modeling parameters and calculation results are presented in Table 1. When the fracture zone lies near the location of the maximum outer bulge development (Figure 12, sections 1 and 2), the fracture zone is reactivated to produce a west facing fault and the bulge topography is significantly modified. In particular, the underriding plate is undeformed (i.e., returned to its unflexed equilibrium configuration) west of the fracture zone, while east of the modeled fracture zone, a short-wavelength topographic high is produced as part of the trench topography (Figure 12, section 2). The form of this topography is produced because of the release of bending stresses and the elastic readjustment of the plate as loads are isolated to the eastern part of the plate. The corresponding modeled gravity shows a 40 mGal amplitude high across the bulge escarpment (Figure 12). When the fracture zone is closer to the trench, the bulge topographic high begins to diminish and eventually disappears due to the progressive loading of the underriding plate by the tip of the overriding plate (Figure 12, section 3). Within approximately 15 km of the trench, the motion along the reactivated fracture zone reverses and the fault escarpment faces the trench (Figure 12, section 4). The corresponding gravity gradient is marked by a sharp increase, the wavelength of which does not represent the actual flexural strength of the underriding plate. For all modeled positions of the fracture zone, the free-air gravity gradient on the outer trench slope is stronger than in the reference model (compare sections 1 and 4 of Figure 12), with its wavelength and amplitude decreasing as the trench is approached.

To illustrate the general applicability of our fracture zone reactivation model, we compare three bathymetric and gravity profiles from across the southern part of the Puysegur ridge/trench system (profiles 1 to 3, Figure 14) with their modeled counterparts. Profiles 1 and 2 were chosen to transect the flat-topped summit of the Puysegur ridge and the L'Atalante fracture zone, while profile 3 was selected to traverse the trench at its maximum depth of -6200 m. At the latitude of profile 1, the modeled fault generates a slope break that mimics the L'Atalante fracture zone topography. The absence of normal faults on the outer trench slope at this latitude is compatible with the relaxation of the bending stresses across the fracture zone. The modeled fault induces a sharp increase of the outer trench slope gravity gradient while reducing both the wavelength and amplitude of the modeled negative gravity anomaly, consistent with the observed free-air gravity anomaly associated with the L'Atalante fracture zone (Figure 14, profile 1 and Table 2).

At the latitudes of profiles 2 and 3 the modeled fault is located farther seaward of the trench. For profile 3 we have estimated the position of the L'Atalante fracture zone located 55 km seaward from the trench. It is necessary to estimate the position of the fracture zone because of the lack of detailed bathymetry data in this area (Figures. 2 and 14, profil 3). The narrow gravity high predicted trenchward of the fault is not observed in the gravity data (Figure 5). This discrepancy can be explain by variations in both the elastic thickness of the underriding plate (*Te*) and the thickness of the overriding plate (T_{load}). We used the same parameters as for profile 2 (Table 2) where the fault is located 35 km seaward from the trench, thus creating a 500-m-high topographic high. We found that a variation of ±2 km of *Te* changes the elevation of the high by 250 m. Similarly, a variation of 1 km of T_{load} changes the elevation of the high by 200 m. Amplitude and wavelength are not significantly modified. Thus, underestimating either *Te* and/or T_{load}, may explain the lack of this topographic high. In terms of the predicted gravity response, it is possible that the fracture zone gravity anomaly is masked by the gravity signature of nearby volcanoes, similar to those mapped in the region of profile 2 (Figure 3). Nevertheless, the slope break observed across the outer trench slope in profile 2 and the corresponding sharp increase in gravity gradient observed in both profiles 2 and 3 suggest that the L'Atalante fracture zone

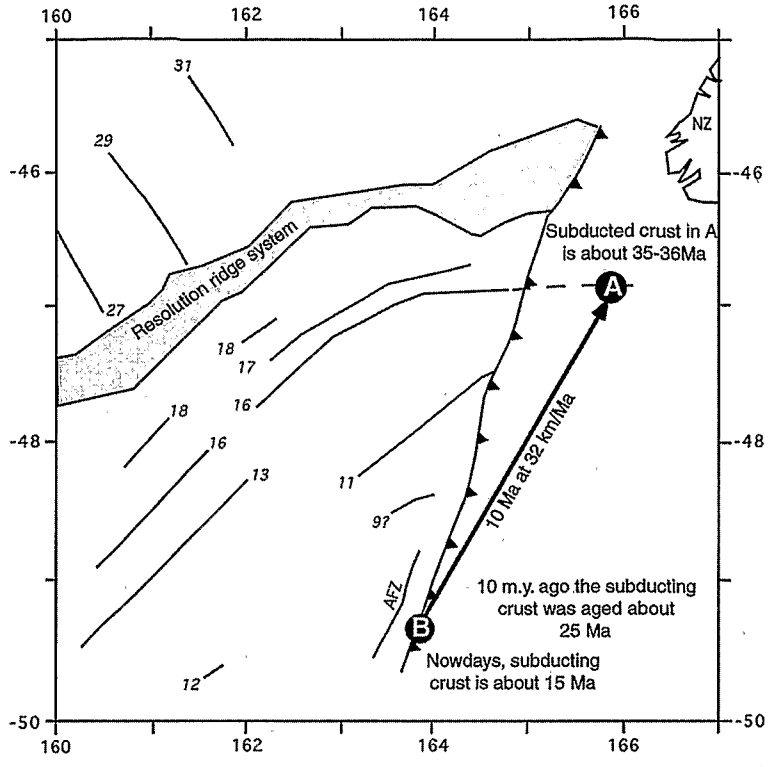

Figure 11. Subduction of the Australian plate has progressively underthrust younger crust beneath the Puysegur ridge with time. Seafloor spreading magnetic anomalies shown in italics [*Wood et al.*, 1996]. Convergence is calculated using finite rotation poles between the Pacific and Australian plates for the last 10 Ma [*Sutherland*, 1995].

has been reactivated as predicted by the models and therefore extends northward to at least the latitude of profile 3 (Figure 14, profiles 2 and 3 and Table 2).

Our model predicts a 40-km increase in the wavelength of the negative gravity anomaly between profiles 1 (35 km) and 3 (75 km), a value that is close to the observed 38 km increase of gravity wavelength (Table 2). Along profile 1 the calculated peak-to-peak amplitude of the gravity anomaly associated with the ridge and trench matches the observed values within 10 mGal. For profiles 2 and 3 the predicted peak to peak amplitudes do not match the observed as well. We believe that these discrepancies are primarily related to local thickening of the ridge related to minor crustal thickness variations of the overriding plate. We conclude that the northward increase of the negative gravity wavelength and amplitude and the strong topographic and gravity gradients across the outer trench slope is a consequence of the flexural reactivation of the L'Atalante fracture zone. As such, this major fracture zone appears to structurally control the Puysegur trench morphology and gravity anomaly.

6.2. Effect of Subducted Fracture Zones Within the Forearc

Previously, we investigated the effect of fracture zone reactivation as they approached the trench. However, the actual subduction of a fracture zone could modify the topography and gravity anomaly of the forearc region within the overriding plate. Figure 13 shows three different static situations for which the modification of the topography and gravity in the forearc region is due to reactivation of a subducted fracture zone. Our modeling indicates that the reactivation of a subducted fracture zones alters drastically the morphology and free-air gravity anomaly of a ridge-trench system. As before, modeling parameters and calculation results are presented in Table 1.

The first-order effect of subducting and reactivating a fracture zone is to segment the load of the overriding plate, thereby reducing the underriding plate deformation as represented by the trench bathymetry (Figure 13). This process induces differential vertical motion in the overriding plate leading to the formation of two topographic summits separated by a trough located above the underthrust fracture zone. The amount of vertical offset and modification to the modeled free-air gravity is function of the fracture zone position relative to the trench. Decreasing the amount of subduction results in shallowing the trench and in increasing the relief between the two summits on the overriding plate (Figure 13, section 1). The free-air gravity of the trench changes dramatically in amplitude and wavelength with the gravity effect of the flexural bulge virtually disappearing. When the distance between the subducted fracture zone and the trench equals the ridge-trench distance (Figure 13, section 3), then the eastern and western summits coalesce into a summit characterized by a steep eastern escarpment and gravity gradient.

We compare three bathymetric and gravity profiles across the northern part of the Puysegur ridge/trench system (profiles 4 to 6 in Figure 14 and Table 2) with superposed modeled topography and gravity obtained using the parameters defined in Table 2. These profiles were selected to sample the regional features of the ridge-trench system (and

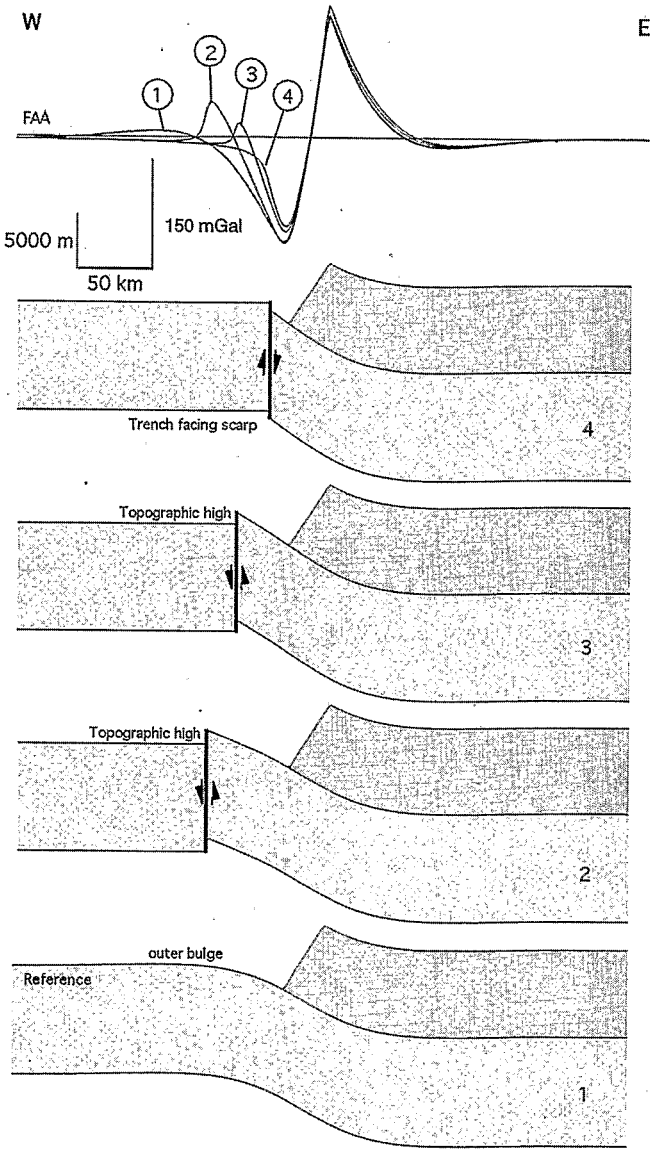

Figure 12. Schematic showing the first-order effects of reactivating fracture zones on the outer trench slope. The flexural bulge is suppressed by relieving the bending stresses of the flexed plate and creating topographic relief between the fracture zone and the trench. The trench free-air gravity anomaly wavelength and amplitude are correspondingly reduced.

the Puysegur Fault) while avoiding local structural complexities. Profile 4 traverses the single-crested Puysegur ridge, profile 5 traverses the double-crested ridge, and profile 6 traverses the southern tip of the New Zealand continental margin where a double-peak free-air gravity anomaly is observed.

At the latitude of profile 4 (Figure 14) the Puysegur Fault extends along the eastern flank of the ridge summit and is marked by an escarpment that is associated with a relatively sharp change in gravity gradient. At this latitude, both the depth of the trench and the free-air gravity anomaly wavelength and amplitude are reduced significantly compared with profile 3. We have modeled these features by introducing a subducted fracture zone beneath the ridge at a distance equal to the observed ridge-trench distance.

Farther north, profile 5 (Figure 14) shows that the Puysegur ridge consists of two, deep summits separated by a trough that is 10 km wide containing approximately 1 km of sediment. The eastern summit of the ridge is flat. Relative to profile 4, the trench is shallower and its free-air gravity wavelength and amplitude are reduced. The free-air gravity associated with the two summits is symmetrical with respect to the trough. We model these observations by introducing a reactivated subducted fracture zone beneath the ridge midway between the trench and the eastern ridge summit. The modeled depth of the trough agrees well with the observed depth (Table 2). However, the calculated gravity over the ridge is too high relative to the observed, and we believe that the adjacent passive margin (the Campbell Plateau) is influencing the

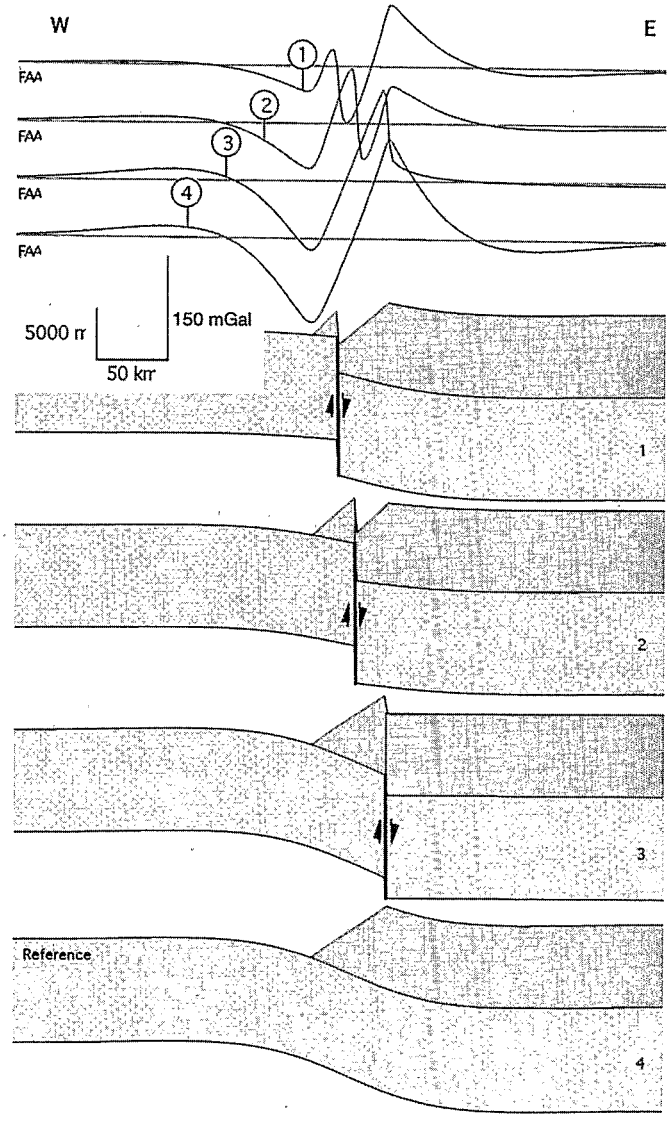

Figure 13. Schematic showing three different static situations of the first-order effects of reactivating a subducted fracture zone within the underriding plate. Fracture zone reactivation segments the load of the overriding plate, thereby inducing differential vertical motion in the forearc region.

Table 2. Measured Values, Parameters, and Results of Calculation for the Six Profiles and Models Presented in Figure 14

					Gravity, mGal						Bathymetry, m				
Profil	*T*load, km	RTD, km	*Te*, km	Fault Position, km Relative to the Trench. (Negative Numbers Westward From the Trench)	West Maximum If So	Central Trough Relative Minimum	Eastward Maximum	Trench Minimum	Amplitude **	Wavelength	Westward Summit If So	Central Trough	Eastward Summit	Trench	Amplitude **
P6					30.0	9.0	53.0	-51	21 ***	?			-400	-4969	-4969
MP6	8	70	24	35	66.0	-56.0	86.4	-60	122 ***	83	2513	-581	2725	-695	3094 ***
UF6	8	70	24				159.0	-135	294	118			3747	-1676	-5423
P5					-9.0	-108.0	-8.0	-106	99 ***	53	-1699	-3632	-1481	-5603	1933 ***
MP5	8	70	23	40	72.3	-53.7	62.4	-70	126 ***	90	2645	-440	2458	-833	3085 ***
UF5	8	70	23				138.0	-120	258	117			3331	-1490	-4821
P4							98.0	-127	225	67			-901	-6067	-5166
MP4	8	60	21	65			125.0	-111	236	102			3448	-1379	-4827
UF4	8	60	21				136.0	-130	266	113			3338	-1633	-4971
P3							64.0	-166	230	70			-1612	-6189	-4577
MP3	8	50	19	-50			136.0	-125	261	75 *			3342	-1655	-4997
UF3	8	50	19				152.0	-133	285	102			3511	-1718	-5229
P2							167.0	-153	320	57			-753	-5726	-4973
MP2	8	40	17	-35			156.0	-115	271	55 *			3548	-1595	-5143
UF2	8	40	17				171.0	-136	307	93			3722	-1820	-5542
P1							207.0	-78	285	32			-155	-5597	-5442
MP1	8	30	15	-20			164.0	-124	288	35 *			3691	-1742	-5433
UF1	8	30	15				180.0	-144	324	87			3853	-2018	-5871

Measured values, P lines (Profile); parameters and results of calculation, MP lines (Modeled Profile). UF lines (UnFaulted) give results for models with the same characteristics than those referred in MP lines, except for the absence of a fault and are used as reference models. For P lines, depth is as observed; however, to compare the "central trough" depth with the calculated one, it is necessary to add at least 1 km due to the presence of sediments in the Puysegur trough (Figure 4). For MP and UF lines, bathymetric zero is set to the average depth of the AUS plate (usually around -4500 m). Thus trench depth is negative and the ridge depth is positive.

*: Wavelength is controlled by the fault position.

**: Amplitude is calculated between the trench minimum and the ridge maximum.

***: Amplitude is calculated between the western summit maximum and the trough minimum.

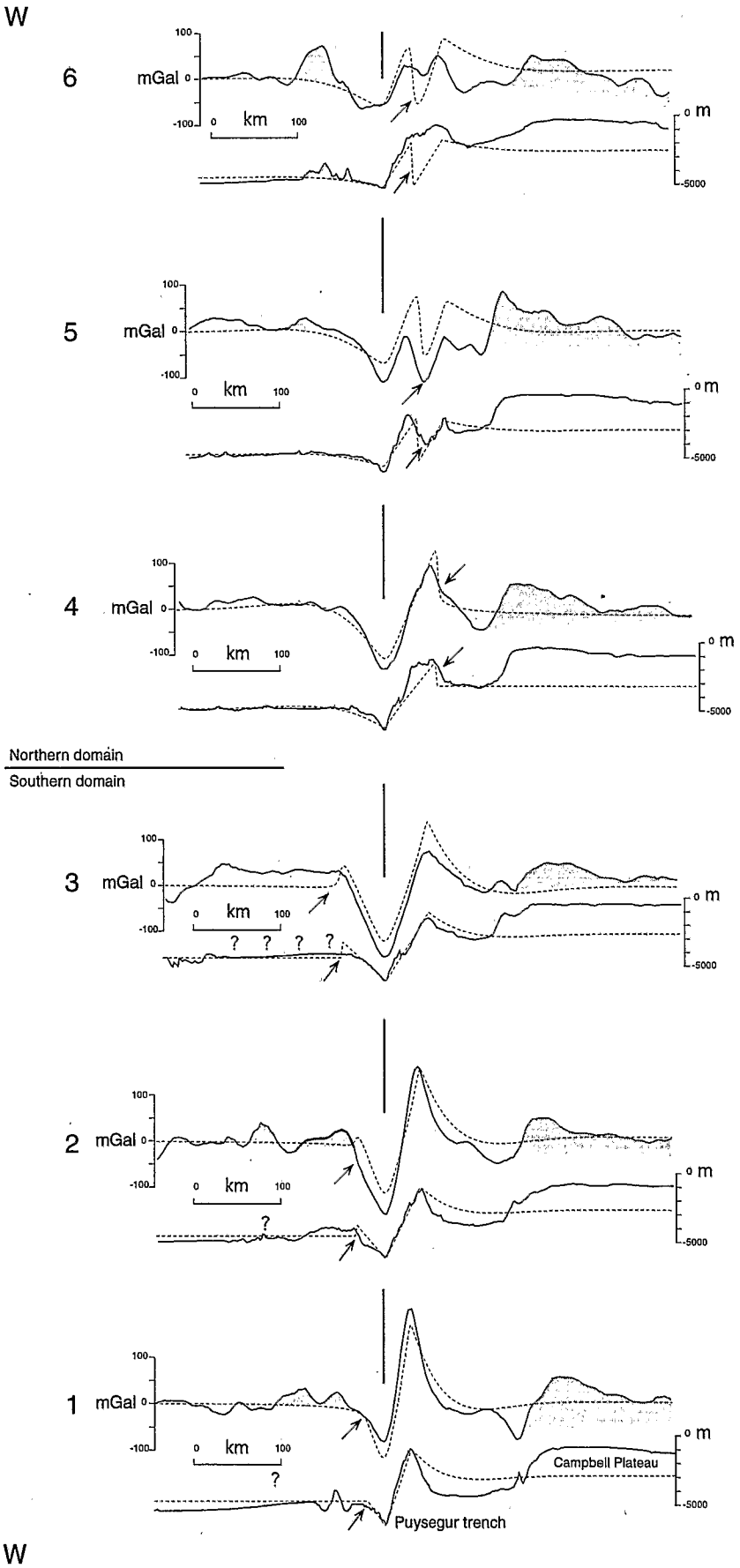

Figure 14. (opposite) Profiles of observed (solid lines) and calculated (dotted lines) topography and free-air gravity anomalies along the Puysegur ridge/trench system. Arrows identify the position of the modeled fault. A question mark is placed where bathymetric data are of poor quality. See Figures. 2 and 5 for location.

form of the gravity anomaly. We will investigate this hypothesis further in the next section.

Reactivating a subducted fracture zone within the underthrust plate also induces ridge subsidence that can be quantified. Including a subducted fracture zone in modeling profile 5 indicates that the eastern summit of the ridge lies about 850 m deeper compared with the equivalent continuous, unfaulted model (Table 2). Therefore the observed 1700-m subsidence of the Puysegur ridge at 47°30'S can be matched by adding the effect of reactivating the subducted fracture zone to the 900 m subsidence calculated as a result of both the ridge broadening and the decrease in plate age being subducted.

For profile 6 (Figure 14) there is no clear morphological trough within the ridge, but the gravity anomaly shows two peaks separated by a 40-mGal low. In modeling this situation we can fit the general free-air gravity wavelength, although the amplitude of the gravity low is too large. A problem also exists with our prediction of an intraridge trough of 2-3 km. We suggest that the trough is filled with sediments, thus explaining the mismatch between the observed and predicted topography and perhaps explaining the low-amplitude gravity anomaly in this region.

In conclusion, our modeling is consistent with the concept that fracture zones on the Australian plate that have been subducted and reactivated beneath the northern part of the Puysegur ridge can modify significantly the morphology of the forearc region. Although our simple kinematic and flexure model does not account for the fault valleys associated with major strike slip fault system (i.e., that of the Macquarie Ridge Complex [*Coffin et al.*, 1994; *Frohlich et al.*, 1997]), this model does account for the double-crested ridge and intervening trough in addition to enhancing the subsidence of the Puysegur ridge. From 48°S northward, shallowing of the trench and associated decrease in the gravity wavelength are clearly compatible with a subducted fracture zone that is closer to the trench in the north than in the south. This interpretation requires that the subducted fracture zone trends slightly oblique to the trench and approximately follows the direction of the Puysegur trough.

6.3. Gravity Effect of the Campbell Plateau Margin

The free-air gravity anomalies over the northern part of the Puysegur ridge are mainly negative (Figure 5). These anomalies are abnormally low when compared to both the southern part of the ridge (Figure 14, profiles 1-3) and our model for profile 5 (Figure 14 profile 5). One possibility to account for this observation is an increased coupling between the underriding and overriding plates. A stronger coupling would increase bending of the overriding plate resulting in a lower gravity anomaly over the ridge.

Alternatively, the free-air gravity over the northern part of the Puysegur ridge could be influenced by the adjacent continental margins of the southern tip of New Zealand and the Campbell Plateau (Figures. 1 and 14). A continental margin usually has a gravity signature characterized by a positive anomaly landward and a negative anomaly seaward, termed the gravity "edge effect." It is thus possible that the negative of this edge effect is contributing to the "excess" negative gravity anomaly of the northern Puysegur ridge. To test this hypothesis, we calculated the gravity effect of the Campbell plateau margin assuming an Airy model of isostasy and removed this gravity effect from the observed free-air gravity anomaly (Figure 15). The gravity edge effect $g(x)$ was

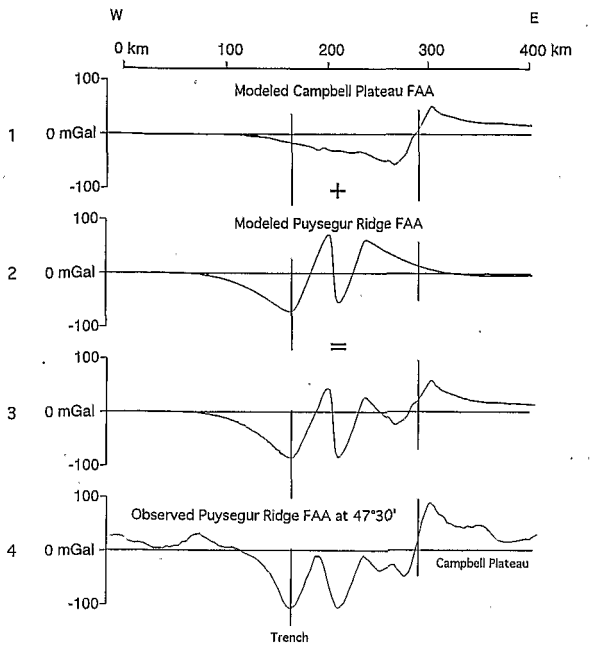

Figure 15. Example illustrating the complicating effects of the Campbell Plateau continental margin on the free-air gravity anomaly of the Puysegur ridge. To mitigate against these complications, we estimate the gravity edge effect of the Campbell Plateau and remove it from the observed gravity. Profile 4 is the same as profile 5 in Figure 14. Gravity anomaly for profiles 1 and 4 returns to zero farther eastward than represented.

calculated using an admittance function approach in which the Fourier transform of the gravity edge effect $G(k)$ is given by

$$G(k) = 2\pi G(\rho_{load} - \rho_w)e^{-kd}\left[1 + e^{-kt_c}\right]H(k) \quad (2)$$

where $H(k)$ is the Fourier transform of the margin topography $h(x)$ (in this case, the Campbell plateau), k is the wave number of the topography, G is the universal gravitational constant, d is the upward continuation distance of the bathymetry, and is the upward continuation distance of the Moho topography.

The resulting anomaly above the ridge is reduced by about 30 mGal (Figure 15, profile 3). Although largely reduced, the predicted anomaly reaches +30 mGal, a value that is still larger than the observed -20 mGal. This discrepancy can result from a 3-D contribution to the gravity from the adjacent continental margin of New Zealand and/or an underestimation of the gravity effect of the Campbell Plateau passive margin; few data are available in this area to constrain its crustal structure. Consequently, we conclude that the negative gravity anomaly associated with the northern part of the Puysegur ridge appears to be mainly related to the adjacent passive margin rather than the subduction process.

7. Geodynamic Implications

7.1. Reconstruction of a Fracture Zone Responsible for the Northern Puysegur Ridge Deformation

Our gravity modeling suggests that the subducted fracture zone trend is slightly oblique to the trench and has a limited geographic distribution. The effects of the reactivation of the

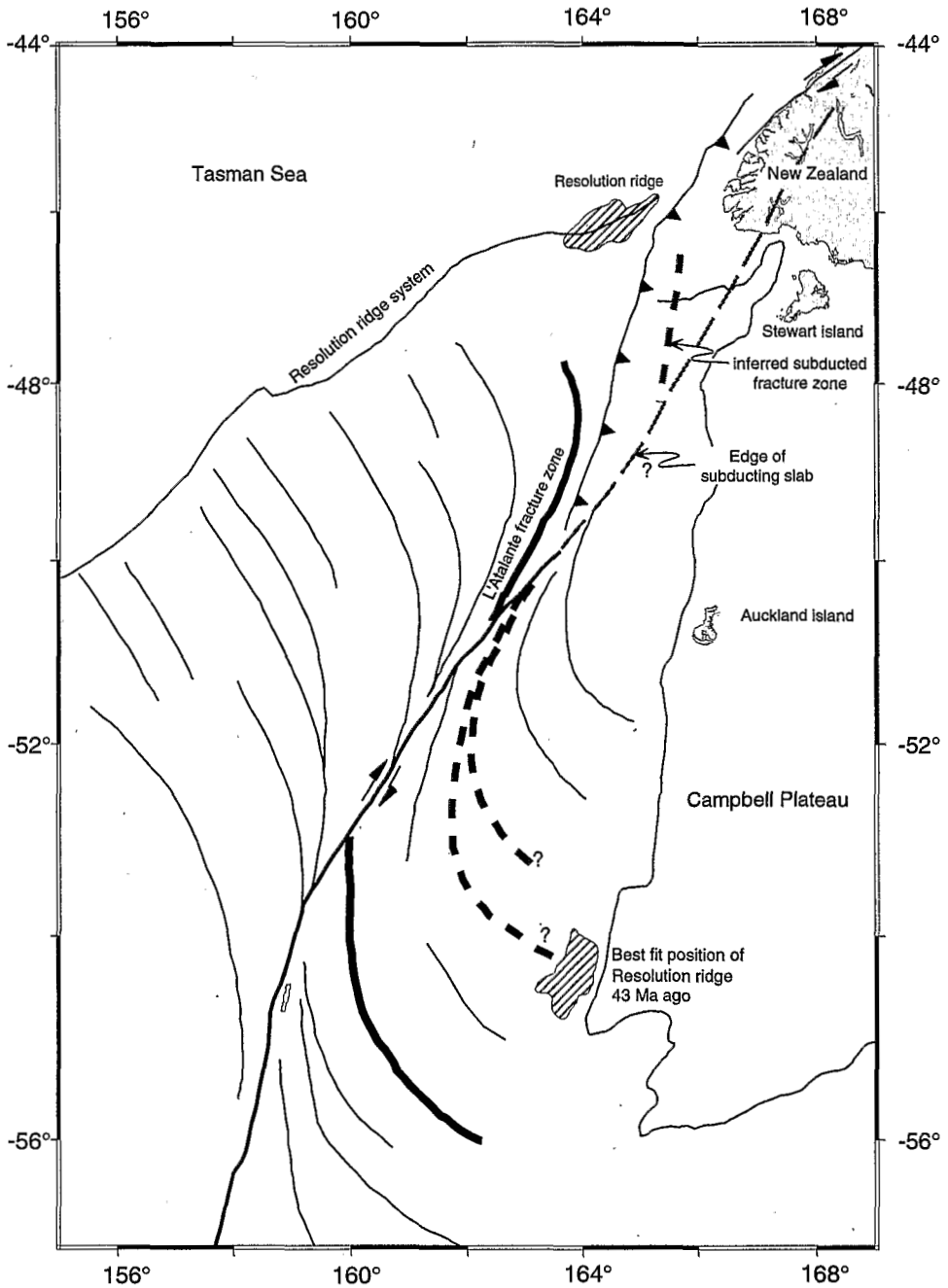

Figure 16. Inferred position of the subducted fracture zone beneath the Puysegur ridge (thick gray dashed line) and its probable southern extension (thick black dashed line). Thick black solid line is the L'Atalante fracture zone and its southern extension based on 330 km of dextral displacement along the strike-slip MacDougall Fault [*Massell et al.*, 1995]. Thin gray dashed line is the surface projection of the extremity of the slab plotted using data from *Davey and Smith* [1983] and *Anderson and Webb* [1994]. Hatched pattern shows the Resolution ridge (RR) and its position 43 m.y. ago when spreading started using the best fit finite rotation poles from *Sutherland* [1995]. Other black thin lines are fracture zones, Campbell Plateau, and Resolution ridge system, all interpreted from the satellite-derived gravity map [*Sandwell and Smith*, 1994]. Medium size line is plate boundary along the MRC.

subducted fracture zone (development of a deep trough flanked by ridge summits, enhanced ridge subsidence, and shallowing of the trench) can be tracked along the ridge summit and adjacent trench segment only north of 48°S and probably up to 46°45'S. South of 48°S the small-amplitude fault valley along the ridge summit would result from strike slip motion along the Puysegur Fault. In this region the absence of the subducted fracture zone effects may indicate that the fracture zone has been subducted without being reactivated to a depth where the Pacific plate is no longer affected by heterogeneities within the underriding Australian plate. Alternatively, and more likely, the subducted fracture zone

may end near 48°S where it merges with the leading edge of the subducted slab (Figure 16). Regional kinematic reconstructions support this interpretation. The sigmoid-shaped fracture zones that formed during the Cenozoic spreading of the South Tasman Sea [*Coffin et al.*, 1994] were dextrally offset along the present-day plate boundary so that each of the two plates carries half, curved fracture zones that asymptotically merge with the plate boundary. A kinematic reconstruction using a 330-km offset [*Massell et al.*, 1995] restores the continuity of the L'Atalante fracture zone across the plate boundary (thick line on Figure 16). This reconstruction indicates that the fracture zones that lay to the east of the L'Atalante fracture zone but on the Pacific plate must have had equivalents on the Australian plate. These fracture zone "ghosts" were likely subducted northeastward at the Puysegur trench. One of these fracture zones appears to be responsible for the forearc deformation of the northern part of the Puysegur ridge (Figure 16).

7.2. Strain Partitioning, Terrane Generation, and Tectonic Erosion

Our analysis has shown that the reactivation of favorably oriented fracture zones is a viable mechanism for deforming the outer bulge and the forearc region of the Puysegur ridge/trench system and thus an important mechanism for modifying convergent margins. Along obliquely convergent margins, reactivating trench-parallel subducted fracture zones may be critical to horizontal strain partitioning, that is, to the development or vertical reactivation of major strike slip faults in the upper plate. Usually, such faults appear in a zone of weakness of the upper plate along or close to a center of active volcanism [*Fitch*, 1972].

In particular, the Puysegur Fault that extends along the summit of the Puysegur ridge trends N26°E and has been interpreted as a possible segment of the strike slip plate boundary before the initiation of subduction [*Collot et al.*, 1995b]. Following the subduction of a fracture zone on the Australian plate beneath the northern part of the ridge, the corresponding segment of the strike slip Puysegur Fault may have undergone vertical adjustments. The resulting N10°E trending Puysegur trough is the best surface expression of the subducted fracture zone. Vertical tectonics induced by reactivating a subducted fracture zone is a process that contributes to the formation and isolation of narrow elongated terranes along obliquely convergent margins.

The escarpment that has been created in the underriding plate beneath the ridge is expected to generate strong basal tectonic erosion (Figure 17). Calculations indicate that this scarp, which can be as high as 3 km (Table 2), is produced because of the partitioning of the overriding plate load as the fracture zone reaches a sufficient depth beneath the ridge to be vertically reactivated. This depth depends on the friction resistance along the fracture zone and the strength of the overriding plate. Conceptually, in a dynamic situation in which a fracture zone is progressively subducted, the related vertical deformation in the upper plate will not evolve from model 1 to model 3 of Figure 13 but will initiate as predicted by one of these models. This vertical deformation requires either to break the upper plate or to reactivate a favorably oriented preexisting fault (e.g., the Puysegur Fault). The resistance of the underriding plate escarpment to ongoing subduction will be strong; thereby it will increase the coupling between the underriding and overriding plates. Because the wedge of upper plate that faces the scarp has been severely tectonized by the subduction process, this wedge can be sheared off and then subducted to greater depth. This transportation will facilitate scarp subduction and will eventually thin the edge of the upper plate by basal tectonic erosion. This process should induce tectonic readjustments in the upper plate making the overlying trough unstable.

8. Conclusions

Recent geophysical investigations of the Puysegur ridge/trench system/Macquarie Ridge Complex provide an excellent opportunity to assess the mechanical implications of subducting trench-parallel fracture zones on the topography and free-air gravity anomaly of the trench and forearc regions using 2-D flexural isostatic models. Reactivating a trench parallel fracture zone that lies a few kilometers seaward from a trench implies a release of the flexural stresses in the downgoing plate. Seaward from the fracture zone, the outer bulge flattens, whereas the slope and the free-air gravity anomaly gradient of the trench outer slope increase. We conclude that the position of the L'Atalante fracture zone with respect to the Puysegur trench controls the

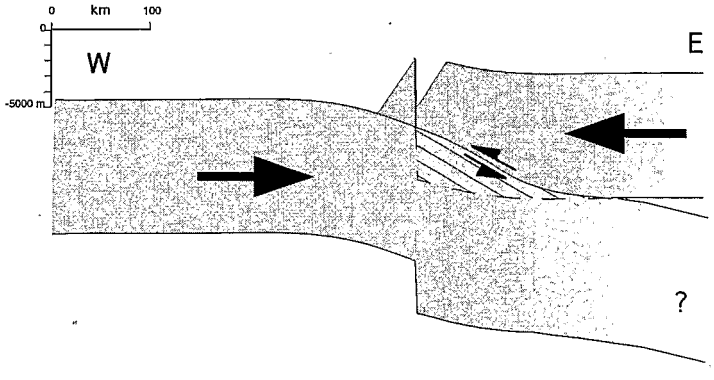

Figure 17. The scarp that has been created in the underriding plate beneath the ridge is expected to generate tectonic erosion of the base of the upper plate because it will oppose ongoing subduction.

morphology of the trench as well as the wavelength and amplitude of the corresponding free-air gravity anomaly.

The subduction and reactivation of a trench parallel fracture zone significantly modifies the topography and free air anomaly of the Puysegur ridge/trench system. Reactivating an underthrusted fracture zone reduces the flexure of the shallow part of the underriding plate. That process diminishes the trench depth and consequently reduces the trench free-air gravity anomaly amplitude and wavelength. The deeper part of the underriding plate subsides to accommodate the isostatic compensation. These vertical movements induce tectonic stresses in the upper plate that could break it or alternatively reactivate preexisting faults as, for example, the northern segment of the strike slip fault along the Puysegur ridge. Further, these vertical motions result in the uplift of the trenchward part of the ridge, and subsidence of the underriding plate, thereby creating the deep Puysegur trough within the ridge above the underthrust fracture zone. Including the effect of an underthrust fracture zone in our model for the Puysegur ridge/trench system, in addition to the effects of the shape of the Puysegur ridge and variations of the elastic thickness of the Australian plate, explains the subsidence of the eastern part of the ridge and the variation of the free-air gravity anomaly over the trench and the ridge. The existence of a fracture zone beneath the ridge is supported by our kinematic reconstruction of the area.

We speculate that reactivating an underthrust fracture zone can facilitate the development of faults in the upper plate that help to accommodate strain partitioning in cases of oblique subduction and thus is conducive to the formation, isolation, and dispersion of elongated terranes. Finally, subducted and reactivated fracture zone will develop a scarp at the base of the upper plate crust that could be responsible for important basal tectonic erosion. Thus trench parallel fracture zones are vertical discontinuities in the oceanic crust that can lead to important margin disruption when subducted.

Acknowledgments. This work was initiated during a visit of J.F.L. to the Lamont-Doherty Earth Observatory (LDEO) and the Institute of Geological and Nuclear Sciences (IGNS). Financial support for this work was provided by l'Institut Francais de Recherche Scientifique pour le Développement en Coopération (ORSTOM), Le Centre National de la Recherche Scientifique (CNRS), and the U.S. National Science Foundation (grant OCE-92-17519). We would like to thank Geoffroy Lamarche and Neal Driscoll for helpful suggestions and critical reviews during the formulation of this research and improving the manuscript, and M. Coffin, G. Moore, and J. Goff, for critically reviewing the manuscript. This work is contribution 161 of UMR-6526 Géosciences Azur CNRS-ORSTOM-UPMC-UNSA and Lamont-Doherty Earth Observatory publication 5775.

References

Anderson, H. J., and T. H. Webb, New Zealand seismicity: Patterns revealed by the upgraded National Seismograph Network, *N.Z.J. Geol. Geophys., 37* (4), 477-493, 1994.

Bandy, W., C. Morteragutierrez, J. Urrutiafucugauchi, and T. W. C. Hilde, The subducted Rivera-Cocos plate boundary: Where is it, what is it, and what is its relationship to the Colima rift?, *Geophys. Res. Lett.*, 22(22), 3075-3078, 1995.

Bodine, J. H., M. S. Steckler, and A. B. Watts, Observation of flexure and rheology of the oceanic lithosphere, *J. Geophys. Res., 86*(B5), 3695-3707, 1981.

Cande, S. C., R. B. Leslie, J. C. Parra, and M. Hobart, Interaction between the Chile ridge and Chile trench: Geophysical and geothermal evidence, *J. Geophys. Res., 92*(B1), 495-520, 1987.

Christoffel, D. A., and W. J. M. Van der Linden, Macquarie ridge - New Zealand Alpine fault transition, in *Antartic Oceanology II: The Australian-New Zealand Sector*, Antarct. *Res. Ser., vol. 19*, edited by D. E. Haynes, pp. 235-242, AGU, Washington, D. C., 1972.

Coffin, M. F., G. D. Karner, and D. A. Falvey, Research cruise yields new details of Macquarie Ridge Complex, *Eos Trans. AGU, 75(48)*, 561-564, 1994.

Collot, J.-Y., et al., Sonic imaging reveals new plate boundary structures offshore New Zealand, *Eos Trans. AGU, 76*(1), 1-5, 1995a.

Collot, J.-Y., G. Lamarche, R. A. Wood, J. Delteil, M. Sosson, J.-F. Lebrun, and M. F. Coffin, Morphostructure of an incipient subduction zone along a transform plate boundary: Puysegur ridge and Trench, *Geology, 23*(6), 519-522, 1995b.

Collot, J.-Y., M. Sosson, J. Delteil, G. Lamarche, R. A. Wood, M. F. Coffin, and J.-F. Lebrun, Subduction initiation and strike slip faulting along the northern Macquarie ridge Puysegur trench (abstract), *Eos tans. AGU, 75*(44), Fall Meet. Suppl., 668, 1994.

Davey, F. J., and E. G. C. Smith, The tectonic setting of the Fiordland region southwest New Zealand, *Geophys. J. R. Astron. Soc., 72*, 23-38, 1983.

Delteil, J., et al., From strike slip faulting to oblique subduction: A survey of the Alpine fault Puysegur trench transition, New Zealand, results of cruise Geodynz-sud leg 2, *Mar. Geophys. Res., 18*(2-4), 383-399, 1996.

DeMets, C., R. G. Gordon, D. F. Argus, and S. Stein, Effect of recent revisions to the geomagnetic reversal time scale on estimates of current plate motions, *Geophys. Res. Lett., 21*(20), 2191-2194, 1994.

Fitch, T. J., Plate convergence, transcurrent faults, and internal deformation adjacent to southeast Asia and the western Pacific, *J. Geophys. Res., 77*(23), 4432-4460, 1972.

Frohlich, C., M. F. Coffin, C. Massell, P. Mann, C. L. Schuur, S. D. Davis, T. D. Jones, and G. D. Karner, Constraints on Macquarie Ridge tectonics provided by Harvard focal mechanisms and teleseismic earthquake locations, *J. Geophys. Res., 102*(B3), 5029-5041, 1997.

Glazner, A. F., and G. Schubert, Flexure of the North American lithosphere above the subducted Mendocino fracture zone and the formation of east-west faults in the transverse ranges, *J. Geophys. Res., 90*(B7), 5405-5409, 1985.

Gunn, R., A quantitative study of isobaric equilibrium and gravity anomalies in the Hawaiian islands, *J. Franklin Inst., 236*, 373-396, 1943.

Kamp, P. J. J., Late Cretaceous-Cenozoic tectonic development of the southwest Pacific region, *Tectonophysics, 121*, 225-251, 1986.

Karner, G. D., et al., Transpressional deformation of the Macquarie ridge complex and its isostatic and topographic implication (abstract), *Eos trans. AGU,75*(44), *Fall Meet. Suppl.*, 668, 1994.

Lamarche, G., J.-Y. Collot, R. A. Wood, M. Sosson, R. Sutherland, and J. Delteil, The Oligo-Miocene Pacific-Australia plate boundary, south of New Zealand: Evolution from oceanic spreading to strike slip faulting, *Earth Planet. Sci. Lett., 148*, 129-139, 1997.

Massell, C., M. F. Coffin, C. Frohlich, P. Mann, C. L. Schuur, and G. D. Karner, Neotectonics of the Macquarie Ridge Complex(abstract), *Eos trans. AGU,76*(45), *Fall Meet. Suppl.*, F581, 1995.

Moore, G. F., and K. L. Sender, Fracture zone collision along the south Panama margin, in *Geologic and tectonic development of the Caribbean Plate Boundary in Southern Central America;*: pp. 201-212, Geol. Soc. of Am., Boulder, Colo., 1995.

Mortimer, N., Geological note: Igneous and sedimentary rocks dredged from the northern Macquarie Ridge, southern Ocean, *J. Aus. Geol. Geophys., 15*(4), 529-537, 1995.

Parker, R. L., The rapid calculation of potential anomalies, *Geophys. J. R. Astron. Soc., 31*, 447-455, 1972.

Reay, A., Andesite from Solander Island, in *Late Cenozoic Volcanism in New Zealand*, edited by I. E. M. Smith, pp. 337-343, R. soc. of N.Z., Wellington, *23*, 1986.

Reyners, M., New Zealand seismicity 1964-87: An interpretation, *N. Z. J. Geol. Geophys., 32*, 307-315, 1989.

Ruff, L. J., J. W. Given, C. O. Sanders, and C. M. Sperber, Large earthquakes in the Macquarie Ridge Complexe: Transitional tectonics and subduction initiation, in *Subduction Zones: Part II*, edited by L. J. Ruff and H. Kanamori, pp. 71-129, Birkhauser-Boston, Cambridge, Mass., 1989.

Sandwell, D. T., and W. Smith, New global marine gravity map/grid based on stacked ERS-1, Geosat and Topex altimetry, *EOS, Trans. AGU, 75(16)*, Spring Meet. Suppl., 321, 1994.

Smith, W. D., Earthquakes at shallow and intermediate depths in Fiordland, New Zealand, *J. Geophys. Res.*, *76*, 4901-4907, 1971.

Stock, J. M., and J. Lee, Do microplates in subduction zones leave a geological record?, *Tectonics*, *13*(6), 1472-1487, 1994.

Summerhayes, C. P., Marine geology of the New Zealand subantarctic sea floor, *rep. 50*, N.Z. dep. of sci. and indus. Res., Wellington, 1969.

Sutherland, R., The Australia-Pacific boundary and Cenozoic plate motions in the SW Pacific: some constraints from Geosat data, *Tectonics*, *14*(4), 819-831, 1995.

Turcotte, D. L., Flexure, in *Advances in Geophysics*, pp. 51-86, Academic, San Diego, Calif., 1979.

Walcott, R. I., Flexure of the lithosphere at Hawaii, *Tectonophysics*, *9*, 435-446, 1970.

Walcott, R. I., Present tectonics and late Cenozoic evolution of New Zealand, *Geophys. J. R. Astron. Soc.*, *52*, 137-164, 1978.

Weissel, J. K., and D. E. Hayes, Evolution of the Tasman Sea reappraised, *Earth Planet. Sci. Lett.*, *36*, 77-84, 1977.

White, R. S., D. Mac Kenzie, and R. K. O'Nions, Oceanic crustal thickness from seismic measurements and rare earth elements inversions, *J. Geophys. Res.*, *97*(B13), 19683-19715, 1992.

Wood, R. A., G. Lamarche, R. H. Herzer, J. Delteil, and B. W. Davy, Paleogene seafloor spreading in the southeast Tasman sea, *Tectonics*, *15*(5), 966-975, 1996.

J.-F. Lebrun, Géosciences Azur, UPMC, B.P. 48, 06235 Cedex, Villefranche sur mer, France. (e-mail: lebrun@faille.unice.fr)

G. Karner, Lamont-Doherty Earth Observatory, Palisades, NY 10964. (e-mail: karner@ldgo.columbia.edu)

J.-Y. Collot, Géosciences Azur, ORSTOM, B.P. 48, 06235 Cedex, Villefranche sur mer, France. (e-mail: collot@ccrv.obs-vlfr.fr)

(Received July 9, 1997; revised December 8, 1997;
accepted December 23, 1997.)